JACS Au
AN OPEN ACCESS JOURNAL OF THE AMERICAN CHEMICAL SOCIETY

pubs.acs.org/jacsau
Article

Ternary Heterostructure Membranes with Two-Dimensional Tunable Channels for Highly Selective Ion Separation

Huiling Liu,[‖] Xin Zhang,[‖] Zixiao Lv, Fang Wei, Qing Liang, Lijuan Qian,* Zhan Li,* Ximeng Chen, and Wangsuo Wu

Cite This: *JACS Au* 2023, 3, 3089−3100
Read Online

ACCESS | Metrics & More | Article Recommendations | Supporting Information

ABSTRACT: Selective ion separation from brines is pivotal for attaining high-purity lithium, a critical nonrenewable resource. Conventional methods encounter substantial challenges, driving the quest for streamlined, efficient, and swift approaches. Here, we present a graphene oxide (GO)-based ternary heterostructure membrane with a unique design. By utilizing Zn^{2+}-induced confinement synthesis in a two-dimensional (2D) space, we incorporated two-dimensional zeolitic imidazolate framework-8 (ZIF-8) and zinc alginate (ZA) polymers precisely within layers of the GO membrane, creating tunable interlayer channels with a ternary heterostructure. The pivotal design lies in ion insertion into the two-dimensional (2D) membrane layers, achieving meticulous modulation of layer spacing based on ion hydration radius. Notably, the ensuing layer spacing within the hybrid ionic intercalation membrane occupies an intermediary realm, positioned astutely between small-sized hydrated ionic intercalation membrane spacing and their more extensive counterparts. This deliberate configuration accelerates the swift passage of diminutive hydrated ions while simultaneously impeding the movement of bulkier ions within the brine medium. The outcome is remarkable selectivity, demonstrated by the partitioning of K^+/Li^+ = 20.9, Na^+/K^+ = 31.2, and Li^+/Mg^{2+} = 9.5 ion pairs. The ZIF-8/GO heterostructure significantly contributes to the selectivity, while the mechanical robustness and stability, improved by the ZA/GO heterostructure, further support its practical applicability. This report reports an advanced membrane design, offering promising prospects for lithium extraction and various ion separation processes.

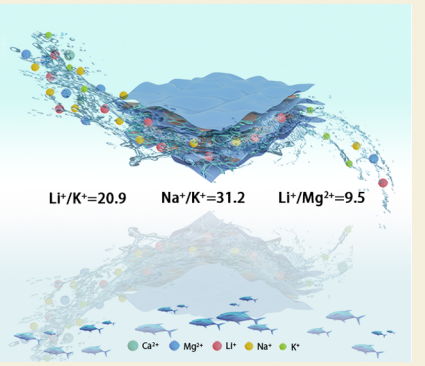

KEYWORDS: *multiple heterojunctions, Salt Lake, lithium extraction, high efficiency separation, graphene oxide membrane*

1. INTRODUCTION

Lithium, being a nonrenewable strategic resource, finds extensive utilization in lithium batteries, aerospace, and nuclear industries owing to its exceptional physical and chemical properties.[1,2] Salt Lake brine stands out as a significant source of lithium, with approximately 60% of lithium compounds extracted from these brines.[3] As a result, the efficient extraction of high-purity lithium ions from Salt Lake brine becomes particularly critical. Present research efforts primarily focus on the separation of lithium and magnesium.[4] However, it is worth noting that the separation between lithium ions and other monovalent ions (sodium, potassium, etc.) receives scant attention.[5,6] Moreover, salt lakes harbor a substantial number of monovalent ions with chemically similar properties and sizes, making their separation more challenging.[7] Hence, achieving effective screening among these monovalent ions is of great significance alongside ensuring efficient separation of lithium and magnesium. Conventional commercial lithium extraction techniques, including calcination impregnation,[8] liquid phase extraction,[9] chemical precipitation, and adsorption,[10] encounter issues such as secondary pollution, high cost, low recovery rate, and poor selectivity.[11] In recent years, membrane technology has garnered increasing attention for extracting lithium from lithium-containing solutions, like seawater and brine lakes, owing to its advantages of low cost, environmental protection, and nonphase transition.[12,13] By offering a more cost-effective and efficient alternative to traditional technologies, membrane technology opens new possibilities for lithium extraction processes.[13,14]

The development of novel membrane materials is of paramount importance for the advancement and application of membrane technology.[15,16] Among these materials, graphene oxide (GO) membrane stands out as an ideal choice due to its outstanding physical and chemical properties, as well as its unique layered structure.[17,18] The ability to adjust the interlayer spacing of the GO membrane allows flexible tuning of the two-dimensional (2D) channels, which plays a key role in realizing the size separation process.[19,20] It has been observed in studies that the hydroxyl and carboxyl groups on

Received: August 13, 2023
Revised: October 24, 2023
Accepted: October 24, 2023
Published: November 10, 2023

https://doi.org/10.1021/jacsau.3c00473
JACS Au 2023, 3, 3089−3100

Scheme 1. Synthesis of G/Z/M Membrane via Zn^{2+}-Induced Confinement in 2D Space

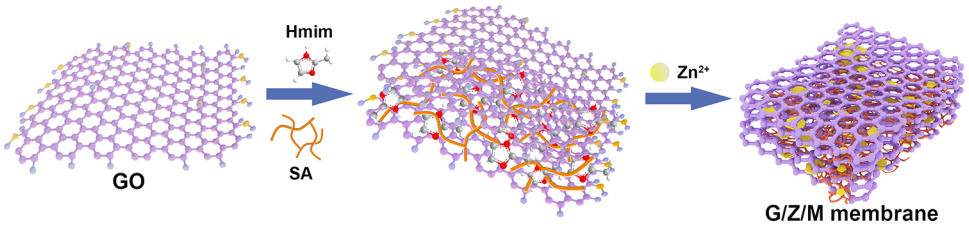

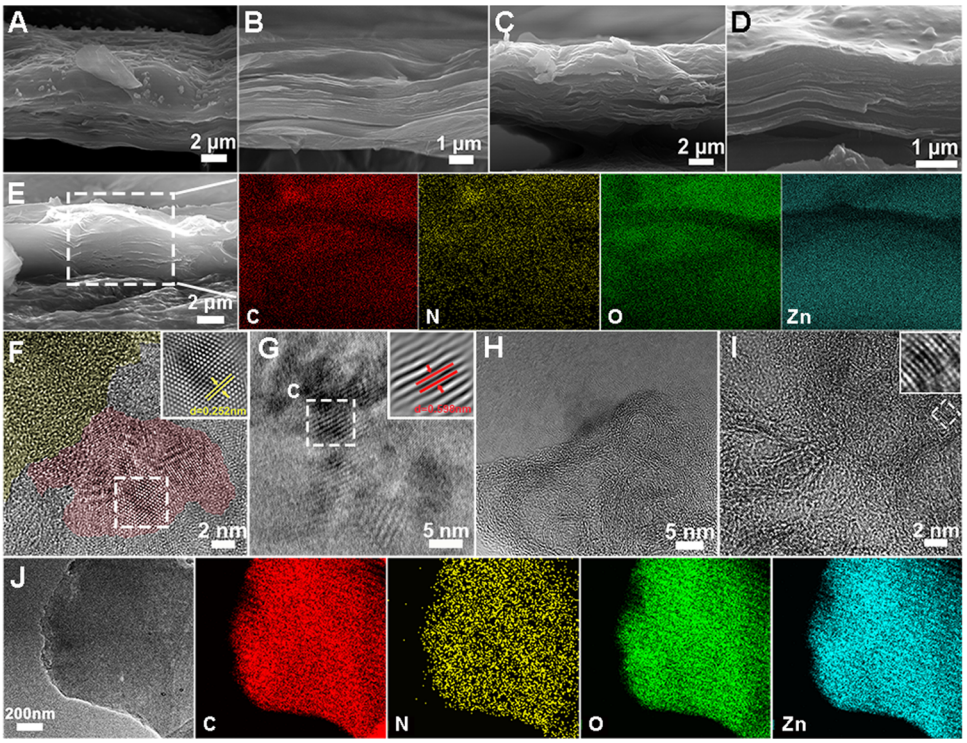

Figure 1. Morphological characterization of the formation of G/Z/M ternary heterojunction membranes. (A, B) SEM images were captured for the cross sections of G/Z/M membranes with different SA additions (G/Z/M-5 and G/Z/M-10). The G/Z/M membranes were named G/Z/M-5 and G/Z/M-10 for SA contents of 5 and 10 wt %, respectively; (C, D) SEM images were captured for the cross sections of G/Z/M membranes, with different Hmim additions (G/Z/M-5 and G/Z/M-10). The G/Z/M membranes were named G/Z/M-a and G/Z/M-b for Hmim contents of 0.82 and 1.35 g, respectively; (E) SEM images of G/Z/M membrane with EDS mapping in the area (marked by white wireframe) and relative intensities of C (red), N (green), O (blue), and Zn (purple) elements; (F) high-resolution transmission electron microscopy (HR-TEM) image of G/Z/M nanosheets containing ZIF-8 and GO heterojunction. The GO and MOF regions are colored yellow and red, respectively. The area within the white wireframe has been magnified and placed in the upper right corner, in which the lattice spacing is marked with yellow words; (G) HR-TEM image of different crystalline surfaces of the G/Z/M nanosheets; the area within the white wireframe has been magnified and placed in the upper right corner, in which the lattice spacing is marked with yellow words; (H) HR-TEM image of G/Z/M nanosheets containing ZA and GO heterojunction; (I) HR-TEM image of G/Z/M nanosheets of ZA nanoribbons; the area within the white wireframe has been magnified and placed in the upper right corner; (J) TEM image of G/Z/M nanosheets and EDS mapping and relative intensities of C (red), N (green), O (blue), and Zn (purple) elements.

GO nanosheets ionize in water, causing the GO nanosheets to acquire negative charges.[21] Consequently, the electrostatic repulsion between these negatively charged nanosheets leads to a loose membrane structure and disordered transport channels, which ultimately reduces the separation efficiency and membrane stability.[22,23] The limitation in question is impeding the practical implementation of GO membranes in industry.[24] Therefore, interlayer modification of GO membranes represents a crucial strategy to fine-tune the interlayer channels and improve membrane selectivity, permeability, and stability.[25] Traditionally, the introduction of three-dimensional (3D) functionalized nanoparticles into GO interlayers inadvertently creates irregular interlayer gaps, leading to distorted ion transport channels and unsatisfactory separation results.[26,27] In contrast, inducing the in situ growth of nanoparticles within the 2D interlayer channels of GO offers an innovative approach. This method ensures the creation of well-structured and flat GO interlayer channels. In addition, the interlayer channels of GO membranes are mainly formed by the stacking of sp^2 regions of graphene oxide sheets at ∼1 nm.[28,29] At such a nanoscale (∼1 nm), the phase behaviors and chemical or physical reactions of substances are different from those at the macroscopic scale (>100 nm).[30−32] Therefore, the confined synthesis of GO membranes at the micro- and nanoscale remains a major challenge.

Based on this, we consider the 2D confinement space of GO nanosheets as a type of nanoreactor, employing a single metal ion cleverly to induce one-step synthesis of a 2D metal−

https://doi.org/10.1021/jacsau.3c00473
JACS Au 2023, 3, 3089−3100

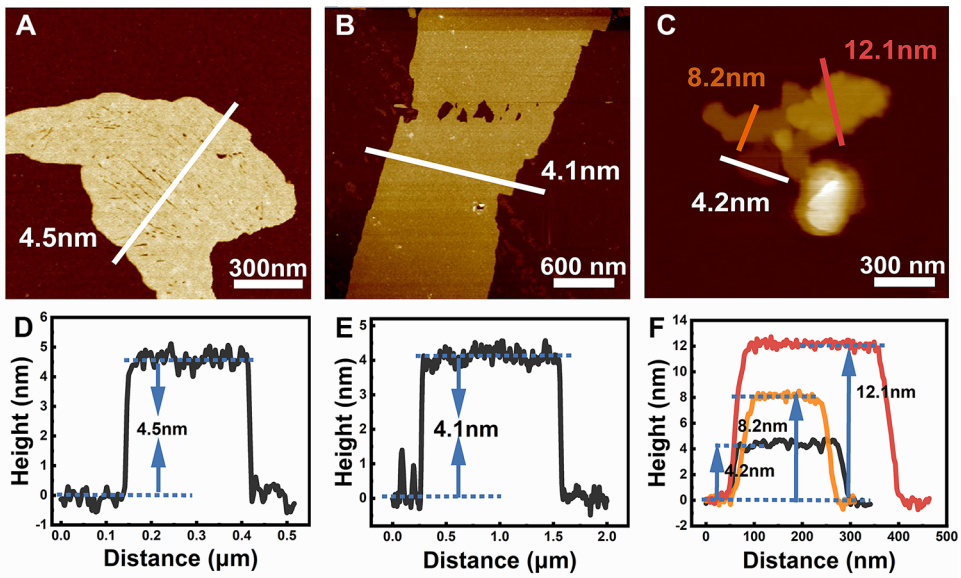

Figure 2. AFM morphology of G/Z/M nanosheets. (A–C) AFM characterizations were conducted on G/Z/M composite membranes with SA additions of 5, 10, and 30 wt %, respectively. Corresponding height profiles were also obtained for these membranes (D–F).

organic framework (MOF) and 2D polymer, resulting in the 2D ternary heterojunction membrane. Among these materials, zeolite imidazolium ester backbone materials, zeolitic imidazolate framework-8 (ZIF-8), with its molecular sieve structure, serves as an excellent choice for alkali metal ion separation due to its angstrom-scale pore window measuring approximately 3.4 Å, a nanoscale pore with a diameter of about 11.6 Å, and an abundance of active sites.[33,34] These features facilitate the rapid transport of ions of specific sizes, leading to improved separation efficiency. In addition, sodium alginate (SA), a linear natural macromolecule with abundant carboxyl and hydroxyl functional groups, has the ability to chelate divalent or multivalent metal ions, resulting in the formation of insoluble hydrogels.[35] By exploiting the bridging effect of these linear molecules, an interlayer connection can be established between adjacent GO nanosheets.[36] This ensures the separation stability of the membrane by contributing to the formation of a stable and highly durable interlayer transport channel.[37] As a result, the resulting 2D ternary heterojunction shows excellent selectivity and stability in the separation of simulated saline, demonstrating significant potential for practical applications.

2. RESULTS AND DISCUSSION

2.1. Preparation of 2D Ternary Heterojunction Membranes

In this study, we simultaneously synthesized 2D ZIF-8 and zinc alginate (ZA) gels in the interlayer of GO membranes by using zinc ion induction. The carboxyl and hydroxyl groups on GO nanosheets have been reported to interact with oxygen-containing functional groups in SA and N in dimethylimidazole (Hmim), allowing these molecules to be retained in large quantities during intercalation of GO membranes.[38,39] Subsequently, the zinc ions penetrate into the intercalation of the GO membranes, where SA and Hmim are coordinated with the zinc ions. In addition, the confined space of the GO membrane layer further limited the three-dimensional growth of ZIF-8 and ZA, resulting in the formation of 2D ZIF-8 and ZA membranes. Therefore, the GO/ZA/MOF (G/Z/M) ternary 2D heterojunction membranes were successfully fabricated as shown in Scheme 1.

2.2. Characterizations of G/Z/M Membranes

First, the morphological analysis of the G/Z/M membranes was carried out by using scanning electron microscopy (SEM). Figure 1A,B shows the cross-sectional images of G/Z/M membranes with different ZA additions. Notably, these images show a distinct layered arrangement resembling a "book-like" structure.[40] In addition, the membrane surface has a uniform texture, similar to that of the GO membrane, which appears relatively flat with no detectable presence of 3D nanoparticles (Figure S1A–C). Figure 1C,D shows the cross sections of G/Z/M membranes with different Hmim additions, demonstrating a well-defined lamination. This observation suggests the presence of MOF and ZA in the form of 2D lamellae positioned between the layers of GO. Moreover, the cross section of the G/Z/M membrane was subjected to elemental analysis using energy-dispersive X-ray spectroscopy (EDX). The data obtained are shown in Figure 1E, which shows the presence of the four constituent elements carbon (C), nitrogen (N), oxygen (O), and zinc (Zn), further confirming the successful synthesis of the ternary G/Z/M membranes.

To obtain further morphological data at the nanoscale, transmission electron microscopy (TEM) was used to observe the G/Z/M nanosheets. Figure 1F shows a high-resolution transmission electron microscopy (HR-TEM) image of the G/Z/M nanosheet. Notably, the nanosheet shows distinct morphological features: the yellow region lacks any lattice striations attributed to the presence of GO, while the red region shows a clear and distinct lattice stripe indicating the presence of 2D ZIF-8. The white box in the upper right corner corresponds to an enlarged section of the lattice stripe, measuring 0.25 nm, which corresponds to the [622] crystallographic plane of ZIF-8.[41] Figure 1G shows a HR-TEM of G/Z/M nanosheets. A lattice stripe with a lattice spacing of 0.59 nm is observed, and comparison with the relevant literature shows that the lattice stripe of 0.59 nm corresponds to the [220] crystal plane of ZIF-8.[42] This evidence supports the existence of a GO/2D ZIF-8

https://doi.org/10.1021/jacsau.3c00473
JACS Au 2023, 3, 3089–3100

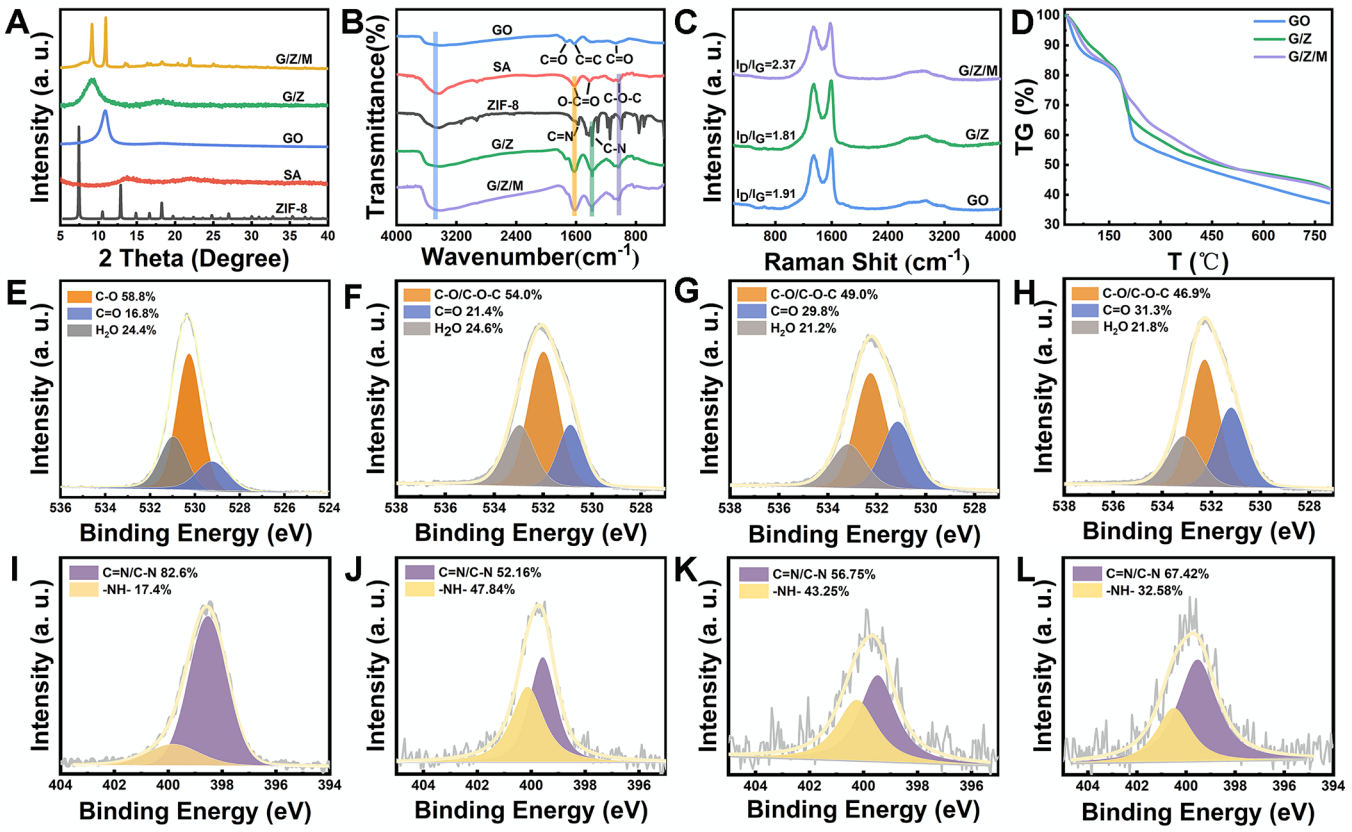

Figure 3. Structural characterization of G/Z/M ternary composite membranes. (A) XRD patterns of ZIF-8, SA, GO, G/Z, and G/Z/M membranes; (B) Fourier transform infrared (FT-IR) spectrum of GO, SA, ZIF-8, G/Z, and G/Z/M membranes, and with indication of major IR peaks; (C) Raman spectrum of GO, G/Z and G/Z/M membranes; (D) thermogravimetric analysis (TGA) patterns GO, G/Z and G/Z/M membranes; (E−H) typical high-resolution X-ray photoelectron spectroscopy (XPS) O1 spectrum of GO, G/Z/M-5, G/Z/M-10, and G/Z/M-30 composite membranes; (I−L) typical high-resolution XPS N1 spectrum of ZIF-8, G/Z/M-a, G/Z/M-b, and G/Z/M-c composite membranes. Note: The membranes are named G/Z/M-5, G/Z/M-10, and G/Z/M-30 for 5, 10, and 30 wt % SA additions, and the membranes are named G/Z/M-a, G/Z/M-b, and G/Z/M-c for 0.82, 1.35, and 1.88 g Hmim additions, respectively.

heterojunction. The HR-TEM image of the G/Z/M nanosheets is further shown in Figure 1H, where curved stripes are clearly visible. These stripes can be attributed to the directional growth of the linear polymer ZA between the GO membrane layers, resulting in the formation of regular banded stripes.[43,44] The white wireframe area in Figure 1I corresponds to a magnified section showing the clearly visible curved stripes, demonstrating the presence of 2D ZA and GO heterojunctions. In addition, Figure 1G provides a TEM image of the G/Z/M nanosheet, showing it as a stack of folded sheets. Nanoscale EDX elemental analysis was also carried out, again revealing a uniform distribution of the four elements C, N, O, and Zn.

Atomic force microscopy (AFM) was used to further study the nanoscale morphology and structure. Figure 2A is the AFM image of the G/Z/M-5 membrane, clearly showing that its thickness is approximately 4.5 nm (Figure 2D). The thickness of the single-layer GO nanosheets we prepared is about 1 nm (Figure S2C,D). Obviously, compared with single-layer GO, the G/Z/M nanosheet layer is thicker. In order to explore the composition of the nanosheets, we used TEM to observe the morphology of the G/Z/M nanosheets (Figure S2F). The surface was relatively smooth and had no wrinkles. For comparison, pure GO nanosheets were observed and found to be very thin and to have many wrinkles (Figure S2E). In addition, the G/Z/M nanosheets were analyzed by EDX and found to contain four elements: C, N, O, and Zn, and they were evenly distributed (Figure 1J). This proves that the thickness of the G/Z/M nanosheets is caused by ZIF-8 and ZA. To further verify this result, we tested the G/Z/M-10 membrane (Figure 2B) and found that the same flakes had a thickness of approximately 4.1 nm and a lateral size of approximately 3.1 μm (Figure 2E). In the G/Z/M-30 membrane (Figures 2C,F and S2A,B), the thinnest sheet still has a thickness of 4.0 nm and is stacked as the smallest unit. Considering the evidence provided by AFM, TEM, X-ray diffraction (XRD), and SEM, it can be concluded that these sheets are composed of GO/ZA/ZIF-8, and we successfully grew 2D ZIF-8 and 2D ZA on GO nanosheets.

Through X-ray diffraction (XRD) analysis, we studied the structural characteristics of the membrane (Figure 3A). In the XRD spectrum of SA, we observed two weak and broad diffraction peaks located at 13.6 and 22.1°, respectively, which indicates that SA is mainly amorphous, consistent with previous research results.[45] The [002] diffraction peak of the pure GO membrane is located at 10.9°, and the corresponding interlayer spacing is 8.2 Å. In the G/Z nanocomposite membrane, after the growth of ZA, the [002] diffraction peak of GO moves to the left to about 9.2°, indicating that the interlayer spacing increases to 9.6 Å. Subsequently, in the G/

https://doi.org/10.1021/jacsau.3c00473
JACS Au 2023, 3, 3089−3100

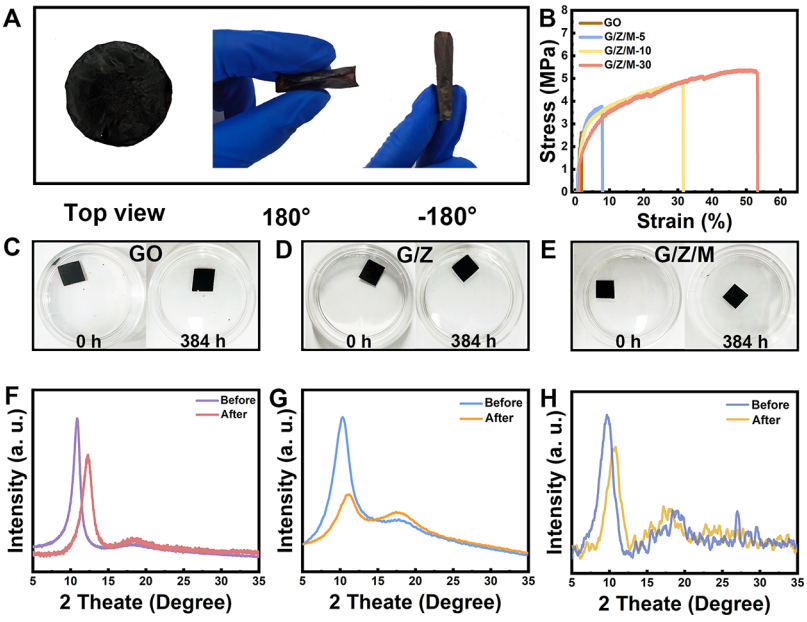

Figure 4. Evaluation of membrane stability and mechanical properties. (A) Images of G/Z/M membranes folding; (B) comparison of tension tests of G/Z/M membranes with different sodium alginate additions; (C–E) comparison photo of GO, G/Z, and G/Z/M membranes before and after being immersed in the solution with pH = 4 after 384 h; (F–H) XRD comparison of GO, G/Z, and G/Z/M membranes immersed in the solution with pH = 4 after 384 h. The membranes are named G/Z/M-5, G/Z/M-10, and G/Z/M-30 for 5, 10, and 30 wt % SA additions.

Z/M membrane, the [002] peak of GO was obviously shifted to 8.1° and the interlayer spacing further increased to 10.8 Å. In addition, the characteristic diffraction peaks of ZIF-8 are also clearly visible.[34] These observations are consistent with the lattice features shown in Figure 1F,G, demonstrating that 2D ZIF-8 and ZA were successfully grown within the interlayer region of the GO membranes. At the same time, the thicknesses of the corresponding GO, G/Z, and G/Z/M membranes also changed. Among them, the thickness of the G/Z/M membrane was the largest due to the growth of 2D ZIF-8 and 2D ZA (Figure S3A–C). In addition, we studied the effects of SA and Hmim ligands on the interlayer spacing of the membrane. As shown in Figure S4, the interlayer spacing of the G/Z/M membrane is located between the GO/SA membrane and the GO/Hmim membrane, which can be attributed to the bridging role of ZA molecules between GO membrane layers.[46]

Analysis by Fourier transform infrared (FT-IR) spectroscopy revealed several prominent absorption peaks in the GO membrane (Figure 3B), including the stretching vibration of −OH at ∼3514 cm^{-1}, the stretching vibration of the carboxyl C═O group at ∼1729 cm^{-1}, the C═C stretching vibration on the sp^2-hybridized carbon chain at ∼1624 cm^{-1}, and the C−O stretching vibration at ∼1066 cm^{-1}, consistent with previous studies.[47] For SA, the stretching vibration peak of −OH was observed at ∼3424 cm^{-1}. In addition, the absorption peaks at ∼1619 and ∼1419 cm^{-1} corresponded to the symmetric and asymmetric stretching vibrations of the carboxyl groups, respectively, with the absorption peak of the C−O−C stretching vibration at ∼1030 cm^{-1}.[48] In ZIF-8, the stretching vibrations of the −OH and N−H groups were observed at ∼3447 cm^{-1}, while the stretching vibrations of the N−C bond in the dimethylimidazole ring were observed at ∼1460 and ∼1423 cm^{-1} and the stretching vibration of C═N was observed at ∼1584 cm^{-1}.[49] For the G/Z composite membrane, characteristic peaks were observed for both GO and SA, with a carbonyl absorption peak for GO at ∼1735 cm^{-1}. Notably, the −OH absorption peak at ∼3514 cm^{-1} in GO was broadened and shifted to ∼3454 cm^{-1}, indicating hydrogen bonding interactions between SA molecules and GO.[50] In the G/Z/M membrane, distinct peaks appeared at ∼1735 cm^{-1}, corresponding to −COOH, and at ∼1033 cm^{-1}, indicating the C−O−C stretching vibration. In addition, the stretching vibration peak of C═N was observed to shift to the right, to ∼1616 cm^{-1}.

Raman spectroscopy was used to provide structural information (Figure 3C). The D and G bands of graphene were observed at ∼1338 and ∼1590 cm^{-1}, respectively, with the intensity ratio (I_D/I_G) between these bands serving as a metric to characterize the degree of disorder in graphene.[51] Comparing the I_D/I_G values of the pure GO membrane with those of the G/Z and G/Z/M membranes, we found them to be 1.81 and 2.37, respectively. These values indicate that the degree of disorder is the highest in the G/Z/M membrane. This observation can be attributed to the growth of ZIF-8 within the interlayer region, as it is likely to introduce additional structural intricates and defects.

The thermal stability of the composite membranes was compared by using thermogravimetric analysis (TGA) (Figure 3D). The initial weight loss at around 100 °C can be attributed to the evaporation of physically adsorbed water molecules. Subsequently, between 100 and 250 °C, the rate of mass loss accelerates, primarily due to the removal of oxygen-containing functional groups and the decomposition of free organic ligands.[52] In the temperature range of 250–500 °C, the carbon chains of GO and SA undergo cleavage, and ZIF-8 begins to decompose, eventually transforming into ZnO with the temperature increase.[53] Notably, it is evident that the thermal stability of the composite membrane is enhanced following the growth of ZA.

X-ray photoelectron spectroscopy (XPS) characterization was conducted to investigate the structure of the composite

https://doi.org/10.1021/jacsau.3c00473
JACS Au 2023, 3, 3089−3100

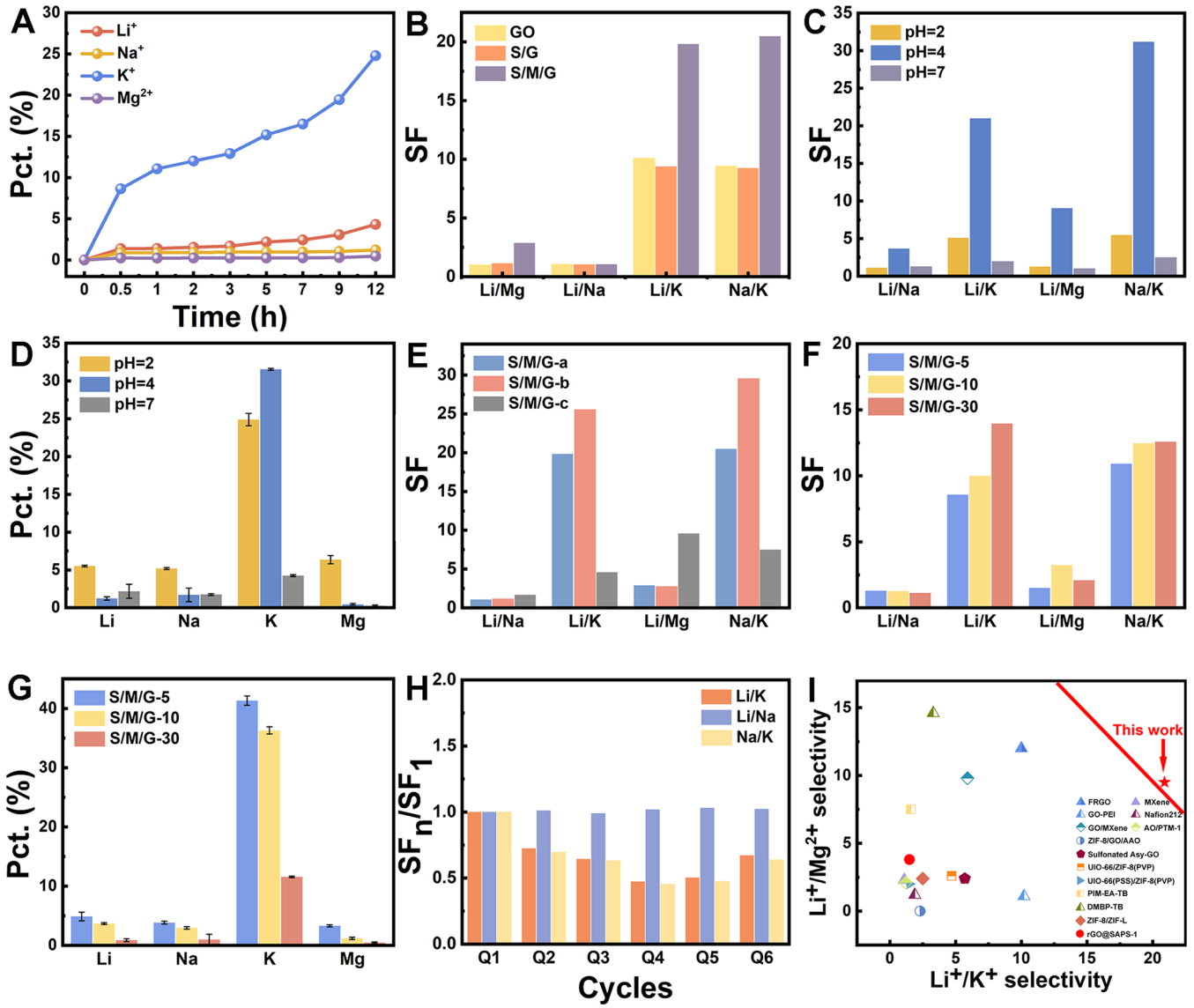

Figure 5. Separation performance of G/Z/M membranes. (A) The permeation percentages (%) of metal ions in simulated Salt Lake water as a function of time and elements; (B) the separation factor (SF) for metal ion selectivity of GO, G/Z, and G/Z/M membranes; (C) separation factors of G/Z/M membranes for simulated Salt Lake water with different acidic conditions; (D) the permeation percentages (pct) of G/Z/M membranes with different acidic conditions; (E) comparison of separation factors of G/Z/M membranes with different Hmim additions; (F) comparison of separation factors of G/Z/M membranes with different SA additions; (G) the permeation percentages (pct) of G/Z/M membranes with different SA additions; (H) separation factors for six-cycle separations using G/Z/M-30-b composite membranes; these sieving experiments were performed in a system that simulates Salt Lake water. Note: All error bars represent the mean standard deviation of three parallel experiments; (I) comparison of Li^+/K^+ and Li^+/Mg^{2+} separation factors of G/Z/M membranes and membranes of the same type.

membrane. Figure S5 presents a comparative analysis of the whole XPS spectrum of the G/Z/M membranes with different SA and MOF additions, revealing the presence of all four elements: C, N, O, and Zn. The C 1s fine spectrum of the composite membrane was further analyzed, with four peaks at 284.6 eV (C−C/C═C), 285.7 eV (C−O−C/C−O), 286.5 eV (C═N/C−N), and 288.2 eV (C═O).[54] Figure 3E displays the O fine spectrum of GO, with C═O in the carboxyl group corresponding to 529.75 eV and C−O in the hydroxyl and alkoxy group at 530.30 eV.[55] In comparison, the binding energy of the O fine spectrum (Figure 3F−H) in the G/Z/M composite membranes increases to 531.12 eV (C═O), 532.25 eV (C−O/C−O-C), and 533.15 eV (H_2O), suggesting an interaction between GO and SA, possibly leading to electron transfer.[56] Moreover, with the increase in the SA content, the C═O content also increases, attributed to changes in the alginate gel content. Furthermore, Figure 3I presents the N fine spectrum of ZIF-8, with C═N/C−N in the imidazole nitrogen at 398.55 eV and a secondary amine in the unliganded imidazole at 399.99 eV.[57] In the G/Z/M composite membranes, the main peak of N shifts leftward to 399.55 eV, indicating an interaction between ZIF-8 and the GO sheet or zinc alginate gel.[58] The C−N/C═N content increases with the increase of the Hmim content, while a decrease in the secondary amine content is observed, which can be attributed to the increased MOF content. Additionally, in the high-resolution XPS spectrum of Zn 2p (Figure S5), two peaks are identified at 1021.8 and 1044.9 eV, corresponding to Zn $2p_{3/2}$ and Zn $2p_{1/2}$, respectively, providing evidence for zinc coordination.

https://doi.org/10.1021/jacsau.3c00473
JACS Au 2023, 3, 3089−3100

2.3. Stability of G/Z/M Membranes

Investigating the long-term stability of the composite membrane and assessing its feasibility for practical industrial applications are of paramount importance. Figure 4A shows that the composite membrane can withstand 180° bending and folding and 180° reverse bending without cracking, indicating its commendable toughness even without support from the substrate membrane. The intercalation of the polymer significantly improves the mechanical properties of the membranes. In order to evaluate this improvement, stress−strain tests were performed on pure GO membranes and G/Z/M membranes with varying amounts of SA. Figure 4B shows that the stress of the pure GO membrane was 2.6 MPa, which increased to 3.7 MPa with 5 wt % SA addition and further increased to 5.4 MPa with 30 wt % SA addition. Correspondingly, the toughness showed a dramatic increase from 21.9 to 227.5 MJ/m^3. This remarkable increase in strength and toughness can be attributed to the growth of ZA within the GO layer, which effectively stabilizes the membrane structure and improves its mechanical properties. The toughness of the G/Z/M membrane was also compared with that of the same type of membrane, showing that the composite membrane has excellent toughness (Figure S6). In addition to mechanical stability, the stability of the separation membranes in an aqueous environment is critical. Therefore, GO membranes (Figure 4C), S/G membranes (Figure 4D), and G/Z/M membranes (Figure 4E) were immersed in an acidic solution of pH 4 for 384 h. As shown in Figure 4C−E, the GO membranes were slightly cracked before and after immersion, while the morphologies of the G/Z and G/Z/M membranes did not change significantly. To further evaluate the structural stability of the composite membranes, we performed XRD analyses (Figure 4F−H). Interestingly, a remarkable phenomenon was observed in all three membranes: the characteristic peak [002] of GO was shifted to the right, indicating that the interlayer distance of the membrane was reduced. This is attributed to the fact that the ionized carboxyl groups (COO^-) in GO are protonated in acidic solutions, leading to a weakening of the electrostatic repulsion between the GO membrane layers and consequently to a decrease in the interlayer distance.[59,60] However, the interlayer distance of G/Z and G/Z/M membranes showed less variation compared to that of pure GO membranes, which was attributed to the hydrogen bonding between SA molecules and GO nanosheets, which made the composite membranes more stable.[61] This property ensures the stability of the composite membranes during the long-term separation process.

2.4. Separation Performance of G/Z/M Membranes

In the separation experiments, simulated brine was prepared according to the Chaika saltlike method for evaluating the separation performance of G/Z/M membranes.[62] The prepared composite membranes were fixed between the feed and drive tanks, with the feed solution being simulated saline lake water and the drive solution being a hydrochloric acid solution of different acidity for osmotic separation (Figure S7A).

First, the permeation kinetics of G/Z/M membranes to simulated Salt Lake water was explored. As shown in Figure 5A, with the prolongation of permeation time, the permeation rate of each ion followed the following trend: $K^+ > Na^+ > Li^+ > Mg^{2+}$, in which it can be clearly seen that potassium ions permeate the fastest, much higher than several other ions, which may be attributed to the fact that potassium ions have the smallest hydration radius (the radius of hydrated ions follows the following rule $Mg^{2+} > Li^+ > Na^+ > K^+$) and are subjected to less size exclusion effect.[63] Preliminary evidence shows that the G/Z/M membranes have a good screening effect on potassium ions in simulated Salt Lake water.

Then, we investigated the effects of GO, G/Z, and G/Z/M membranes on the separation performance of simulated saline lake water, respectively. As shown in Figure 5B, the separation effects of pure GO and G/Z membranes showed a similar trend, with the separation factor of $Li^+/K^+ \approx 9.5$ and the $Na^+/K^+ \approx 9.3$. However, when the performance of the G/Z/M membranes was evaluated, a striking phenomenon was found. Its separation efficiency was significantly improved, with the $Li^+/K^+ \approx 25.1$ and the $Na^+/K^+ \approx 29.5$. It was first demonstrated that the G/Z/M heterojunction membrane had a good effect on the separation of metal ions in simulated saline lake water. The effects of different separation conditions on the separation performance were then investigated.

Furthermore, the influence of the pH of the drive fluid on the permeation of salt ions was examined (Figure 5C). Surprisingly, it was noted that as the pH in the drive tank decreased, the permeation of ions exhibited an upward trend. This observation aligns with the corresponding permeation data illustrated in Figure 5D. This behavior can be attributed to the heightened concentration difference of protons between the feed tank and the drive tank, consequently intensifying the driving force responsible for ion transport. However, it is important to consider that although increased permeability leads to enhanced ion transfer, it also inevitably leads to a decrease in the separation factor. Consequently, a drive fluid with a pH = 4 was determined to be the optimal choice for achieving the desired separation performance.

The effect of varying the MOF content on the separation performance was investigated (Figure 5F). Interestingly, it was observed that when the MOF content was increased from a to b, the permeability of potassium ions increased, while the permeability of other ions decreased. When the MOF content was further increased to c, the ionic permeability decreased (Figure S7b). Among them, the G/Z/M-b membrane showed the highest separation factor, and the best separation of simulated saline lake water was achieved by the prepared G/Z/M membrane when the addition of Hmim was 1.35 g (Figure 5F).

The effect of SA addition on the separation process was also investigated. It was observed that the overall separation experienced a slight improvement as the content of SA increased (Figure 5F). However, the increase in polymer content resulted in a decrease in the ionic transmittance (Figure 5G). Interestingly, the most favorable separation performance was achieved when employing a 30 wt % SA concentration. To investigate the cyclic separation stability of the composite membrane, the optimal ratio of G/Z/M membrane was employed for consecutive separation cycles mimicking Salt Lake brine (Figure 5H). Each cycle encompassed a duration of 12 h, and after a total of six cycles, the separation factor of Li^+/Na^+ remained essentially unchanged, and it was observed that the separation efficiency of Li^+/K^+ and Na^+/K^+ remained above 50%. This finding signifies the membrane's promising capability to effectively and steadily separate monovalent ions present in simulated Salt Lake brine. To further assess the structural stability of the membrane following six separation cycles, XRD tests were

https://doi.org/10.1021/jacsau.3c00473
JACS Au 2023, 3, 3089−3100

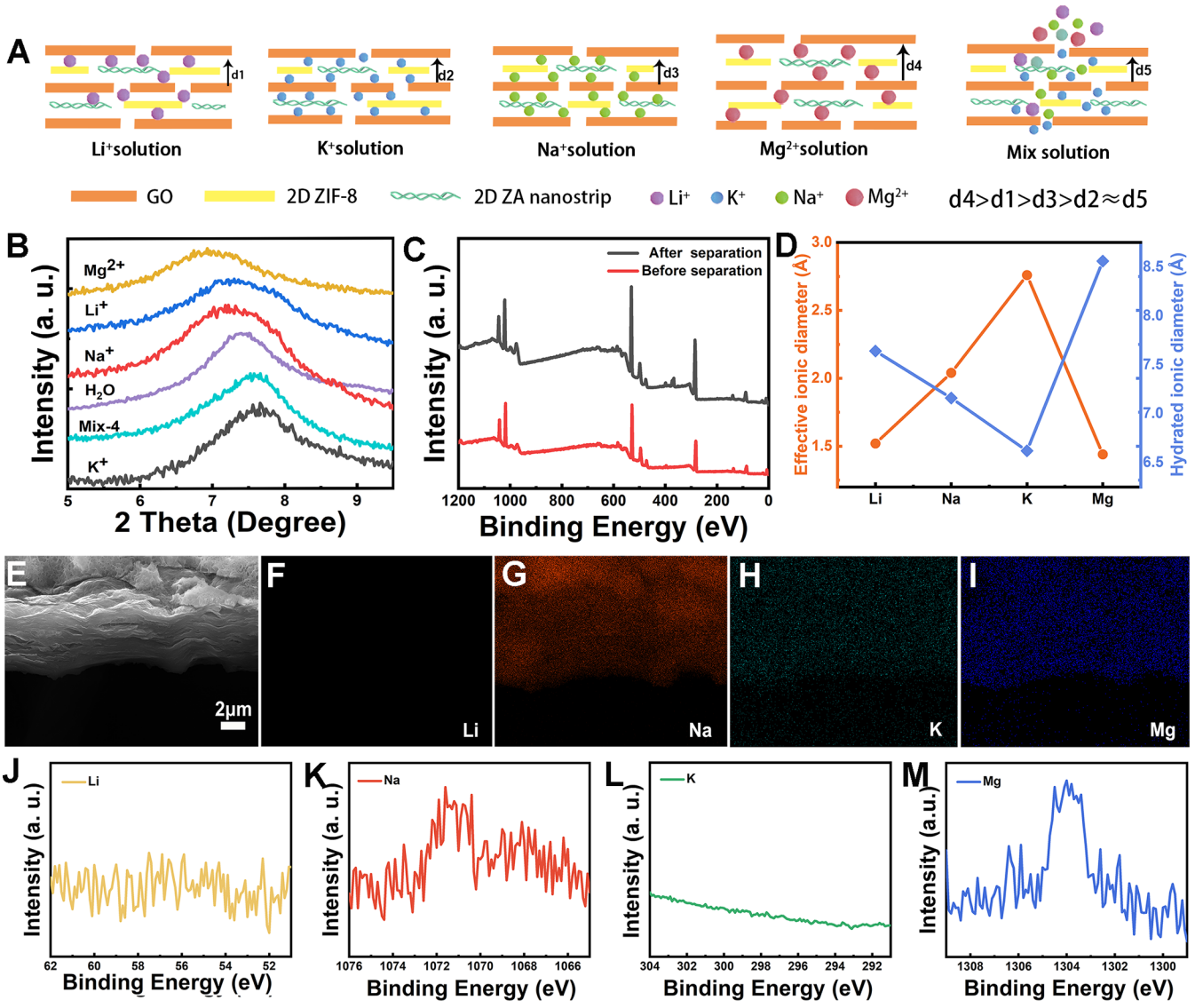

Figure 6. Separation mechanisms of G/Z/M membranes. (A) Schematic representation of the change in layer spacing when G/Z/M membranes are immersed in different ionic solutions, respectively; (B) comparison of XRD of G/Z/M membranes when immersed in different ionic solutions, respectively; (C) comparison of XPS full spectra of G/Z/M membranes before and after separation; (D) effective ionic and hydrated ionic diameters; (E) cross section of the separated G/Z/M membranes; (F–I) distribution of EDX elements in the cross section of the separated G/Z/M membranes; (J–M) XPS fine spectra of separated G/Z/M membranes.

conducted (Figure S7C). The analysis demonstrates that the distinctive [002] characteristic peak of GO in the G/Z/M membrane experienced only a slight shift from 8.5 to 8.2 Å before and after the separation process. This means that the membrane exhibits good structural stability and ensures a consistent and stable separation. In addition, the Li^+/Mg^{2+} and Li^+/K^+ separation factors of G/Z/M membranes were also compared with those of the same type of membranes, and the separation performance of G/Z/M was far superior to that of the same type of separation membranes, as shown in Figure 5I.[33,64−72]

2.5. Separation Mechanisms of G/Z/M Membranes

In the membrane separation process, the size sieving effect and the interaction between the functional groups within the channels between the membrane layers and the target sieving substances play a crucial role in the separation performance.[73] Previous separation experiments indicated that the permeation rate order of each ion was $K^+ > Li^+ > Na^+ > Mg^{2+}$ (Figure 5B,E,G). It has been reported that the hydrated ion diameter of these ions follows the order K^+ (6.62 Å) < Na^+ (7.16 Å) < Li^+ (7.64 Å) < Mg^{2+} (8.56 Å) (Figure 6D). This indicates that the permeation process of the G/Z/M membrane is largely controlled by the size exclusion effect. To further investigate the separation mechanism, the G/Z/M membranes were soaked in 0.25 M NaCl, LiCl, KCl, and $MgCl_2$ solutions, respectively. After removal of the salt solutions, the G/Z/M membrane was subjected to an XRD test. As shown in Figure 6B, the interlayer spacings were significantly shifted compared to the membranes soaked in pure water, indicating that the interlayer channels of the G/Z/M membrane are tunable and that ions of different sizes cause different interlayer spacings. The order from smallest to largest spacing is $K^+ < Na^+ < Li^+ < Mg^{2+}$, which is consistent with the hydrated ionic size and confirms previous literature reports.[74] However, when the G/Z/M membrane was immersed in a mixed solution system containing lithium, sodium, potassium, and magnesium ions,

https://doi.org/10.1021/jacsau.3c00473
JACS Au 2023, 3, 3089−3100

an interesting phenomenon was observed. The interlayer distance in the mixed system was slightly larger than that for potassium ions alone but smaller than the interlayer distance observed when Na^+, Li^+, and Mg^{2+} were soaked (Figure 6A,B). Therefore, it is found that the interlayer channels of the G/Z/M membrane can allow potassium ions to pass through in the mixed system while excluding sodium, lithium, and magnesium ions (Figure 6A). In addition, the cross section of the separated G/Z/M membranes observed by SEM revealed that the membrane layer structures were tightly laminated (Figure 6E), further confirming the excellent stability of the composite membranes. EDX elemental analysis (Figure 6F–I) shows that the content of potassium and lithium ions is minimal, while the content of sodium and magnesium ions is relatively higher. This difference can be attributed to the higher permeation rate of potassium and lithium ions, leading to greater permeation through the membrane layers. As a result, potassium and lithium ions are less retained in the interlayer of the membrane. On the other hand, sodium and magnesium ions have a lower permeability, resulting in some of them being retained in the interlayer, possibly due to interactions between the ions and the functional groups. Similarly, the G/Z/M membranes were subjected to XPS characterization before and after separation (Figure 6C,J–M), and the fine spectra of the separated membranes show results consistent with the EDX analysis from SEM. In conclusion, the separation of G/Z/M membranes in simulated saline lake water depends primarily on the size screening effect. The size of the interlayer channels in the G/Z/M membranes in the mixed system is controlled by the presence of potassium ions, allowing the interlayer channels to be slightly larger than the hydration diameters of potassium ions and facilitating the rapid passage of potassium ions.

3. CONCLUSIONS

In this work, 2D ZIF-8 and 2D ZA were synthesized simultaneously within the interlayer of the GO membrane for preparing a novel 2D ternary heterojunction membrane. Remarkably, the introduction of a 2D MOF significantly enhanced the ion separation selectivity of the membranes. Experimental results showed separation selectivity values of about K^+/Li^+ = 20.9, Na^+/K^+ = 31.2, and Li^+/Mg^{2+} = 9.5, respectively. In addition, incorporation of the polymer between the GO layers effectively improved the mechanical properties and stability of the heterojunction membrane. Overall, the success of this study in synthesizing the 2D ternary heterojunction membrane and revealing its enhanced selectivity for ion separation highlights promising possibilities for advancing membrane technology. The combination of environmentally friendly methods and the investigation of novel interlayer structures within GO offers significant contributions to the design and preparation of advanced 2D membranes.

4. MATERIALS AND METHODS

4.1. Materials

Sulfuric acid (H_2SO_4) (96–98 wt %) was purchased from Sichuan Longxi Science Company. Hydrochloric acid (HCl) (36–38 wt %) and potassium permanganate ($KMnO_4$) were purchased from Chengdu Kolon Chemical Company. Graphite flakes and lithium chloride (LiCl) were purchased from Aladdin Chemical Reagent Company. Sodium alginate (SA) was purchased from Shanghai Maclean. Sodium chloride (NaCl), potassium chloride (KCl), calcium chloride ($CaCl_2$), sodium nitrate ($NaNO_3$), hydrogen peroxide (H_2O_2) (30 wt %), and zinc nitrate hexahydrate ($Zn(NO_3)_6{\cdot}H_2O$) were purchased from Tianjin Damao Chemical Reagent Factory. Dimethylimidazole (Hmim) was purchased from Shanghai Zhan yun Chemical Company. All of the reagents used in the experiments were analytically pure and were not purified before use. The water used for the experiments was 18.2 MΩ/cm ultrapure water.

4.2. Synthesis of Graphene Oxide (GO)

This paper was prepared with reference to the modified Hummers method as follows.[75] Slowly add 150 mL of concentrated sulfuric acid, 5 g of 100 mesh flake graphite, and 2.5 g of $NaNO_3$ to a 500 mL three-necked flask. Place the flask in an ice–water bath with mechanical stirring and maintain the temperature at about 4 °C. Then very slowly add 20 g of potassium permanganate, keeping the temperature below 4 °C. Then very slowly add 20 g of potassium permanganate, keeping the temperature below 4 °C throughout. After the addition, start time, mechanical stirring for 2 h. After the low-temperature reaction, replace the ice water bath with a warm water bath, control the reaction temperature to 35–40 °C, and continue mechanical stirring for 24 h. After the medium temperature reaction, slowly add 100 mL of ultrapure water, small amounts of drops into the flask, and the temperature during the addition of water should not exceed 60 °C. After adding the ultrapure water, heat to a temperature of about 90 °C for 15 min, stop heating and pour the reacted slurry into a beaker containing 1 L of water. Slowly add hydrogen peroxide (30%) until there are no more bubbles and the slurry turns golden yellow. Allow to stand for 12 h and discard the supernatant. Wash with 15% hydrochloric acid or pure water and centrifuge until the supernatant is neutral. Transfer to a wide-necked flask.

4.3. Synthesis of Ternary G/Z/M Membrane

First, the prepared graphene oxide (GO) solution was diluted to 0.5 g/L and then sonicated for 2 h to obtain a homogeneous GO solution. A 0.02 g/L sodium alginate (SA) solution was prepared. To 12 mL of 0.5 g/L aqueous GO solution, 5 wt % of 0.02 g/L SA solution and 0.82 g of Hmim were added and stirred for 6 h at room temperature to ensure adequate mixing. A 0.22 μm microporous poly(ether sulfone) membrane was then used as a substrate, and the mixed solution was filtered under vacuum to obtain the SA/Hmim/GO membrane. The membrane was dried at room temperature for 12 h. The membrane was immersed in 100 mL of 2 wt % zinc nitrate solution and left at room temperature for 6 h to cross-link the zinc ions with sodium alginate and coordinate with dimethylimidazole. Finally, the membrane was repeatedly rinsed with pure water to remove excess impurities such as ZIF-8 and zinc ions and dried at room temperature for 12 h. When the mass of the composite membrane remained unchanged upon weighing, drying was defined as complete, and the two-dimensional G/Z/M heterogeneous junction membrane was obtained.

4.4. Synthesis of G/Z/M Membranes with Different Ratios

The effect of the MOF on membrane properties was investigated by adjusting the amount of dimethylimidazole, as the amount of dimethylimidazole directly affects the amount of 2D MOF produced. The amounts of dimethylimidazole were 0.82, 1.35, and 1.88 g, respectively. The prepared membranes are named G/Z/M-a, G/Z/M-b, and G/Z/M-c.

The effect of the polymer on the membrane properties was also investigated by adjusting the amount of sodium alginate as the amount of sodium alginate directly affects the amount of 2D zinc alginate gel (ZA) produced. The amounts of sodium alginate were 5, 10, and 30 wt %, respectively. The prepared membranes are named G/Z/M-5, G/Z/M-10, and G/Z/M-30.

4.5. Separation Result Calculation

The prepared G/Z/M membrane was used to separate the Li^+, Na^+, K^+, and Mg^{2+} ion mixture solution, and the samples were analyzed by inductively coupled plasma optical emission spectroscopy (ICP-OES) for the concentration of each ion and the permeation percentages (Pct) was calculated using the following equation.[76]

https://doi.org/10.1021/jacsau.3c00473
JACS Au 2023, 3, 3089–3100

$$\mathrm{Pct}=\frac{C_t}{C_0} \quad (1)$$

where C_t is the measured concentration of the metal ion in ppm and C_0 is the concentration of the starting ion of the permeate.

The separation factor is calculated using eq 2 based on the ratio of permeability.[77]

$$\mathrm{SF}=\frac{\mathrm{Pct}_{(\mathrm{J})}}{\mathrm{Pct}_{(\mathrm{M})}} \quad (2)$$

where SF is the separation factor, $\mathrm{Pct}_{(\mathrm{J})}$ and $\mathrm{Pct}_{(\mathrm{M})}$ are the permeation percentages calculated from eq 1, with $\mathrm{Pct}_{(\mathrm{J})} > \mathrm{Pct}_{(\mathrm{J})}$.

Please refer to the Support Information for more specific information.

■ ASSOCIATED CONTENT

Data Availability Statement

The authors declare that the data supporting the findings of this study are available within the article and the Supporting Information. All other data are available from the lead contact on reasonable request.

Supporting Information

The Supporting Information is available free of charge at https://pubs.acs.org/doi/10.1021/jacsau.3c00473.

Experimental details such as preparation method, instrument type, details of separation experiments, other characterization of G/Z/M membranes, membrane properties, etc.; additional figures (Figures S1–S7) (PDF)

■ AUTHOR INFORMATION

Corresponding Authors

Lijuan Qian − *MOE Frontiers Science Center for Rare Isotopes, Lanzhou University, Lanzhou 730000, China; School of Nuclear Science and Technology, Lanzhou University, Lanzhou 730000, China;* orcid.org/0000-0001-9457-247X; Email: qianlj@lzu.edu.cn

Zhan Li − *MOE Frontiers Science Center for Rare Isotopes, Lanzhou University, Lanzhou 730000, China; School of Nuclear Science and Technology, Lanzhou University, Lanzhou 730000, China;* orcid.org/0000-0001-7748-2691; Email: liz@lzu.edu.cn

Authors

Huiling Liu − *MOE Frontiers Science Center for Rare Isotopes, Lanzhou University, Lanzhou 730000, China; School of Nuclear Science and Technology, Lanzhou University, Lanzhou 730000, China*

Xin Zhang − *MOE Frontiers Science Center for Rare Isotopes, Lanzhou University, Lanzhou 730000, China; School of Nuclear Science and Technology, Lanzhou University, Lanzhou 730000, China*

Zixiao Lv − *MOE Frontiers Science Center for Rare Isotopes, Lanzhou University, Lanzhou 730000, China; School of Nuclear Science and Technology, Lanzhou University, Lanzhou 730000, China*

Fang Wei − *MOE Frontiers Science Center for Rare Isotopes, Lanzhou University, Lanzhou 730000, China*

Qing Liang − *CAS Key Laboratory of Chemistry of Northwestern Plant Resources and Key Laboratory for Natural Medicine of Gansu Province, Lanzhou Institute of Chemical Physics, Chinese Academy of Sciences, Lanzhou 730000, China*

Ximeng Chen − *MOE Frontiers Science Center for Rare Isotopes, Lanzhou University, Lanzhou 730000, China; School of Nuclear Science and Technology, Lanzhou University, Lanzhou 730000, China*

Wangsuo Wu − *MOE Frontiers Science Center for Rare Isotopes, Lanzhou University, Lanzhou 730000, China; School of Nuclear Science and Technology, Lanzhou University, Lanzhou 730000, China*

Complete contact information is available at: https://pubs.acs.org/10.1021/jacsau.3c00473

Author Contributions

‖H.L. and X.Z. contributed equally to this work. H.L. and X.Z. conceived the project. Z.L., L.Q., X.C., and W.W. supervised the project. H.L., Z.L., and F.W. performed the experiments and characterizations. H.L. and Q.L. carried out AFM testing and analyzed the data. H.L., X.Z., Z.L., and L.Q. cowrote the manuscript. All authors discussed the results and commented on the manuscript.

Notes

The authors declare no competing financial interest.

■ ACKNOWLEDGMENTS

This work was supported by the National Natural Science Foundation of China (Nos. 22076071, 21974146, 12105130), the Fundamental Research Funds for the Central Universities (lzujbky-2023-stlt01, lzujbky-2021-ct19, lzujbky-2021-sp34, and lzujbky-2022-sp03), and the Opening Fund of Hubei Key Laboratory of Bioinorganic Chemistry and Materia Medica (No. BCMM202202), and the Research on Comprehensive Helium Extraction Process from Natural Gas and Supporting Technologies (22ZY2QM001).

■ REFERENCES

(1) Ebensperger, A.; Maxwell, P.; Moscoso, C. The lithium industry: Its recent evolution and future prospects. *Resour. Policy* **2005**, *30* (3), 218–231.

(2) Meng, F.; McNeice, J.; Zadeh, S. S.; Ghahreman, A. Review of Lithium Production and Recovery from Minerals, Brines, and Lithium-Ion Batteries. *Miner. Process. Extr. Metall. Rev.* **2021**, *42* (2), 123–141.

(3) Guo, Y.; Ying, Y.; Mao, Y.; Peng, X.; Chen, B. Polystyrene Sulfonate Threaded through a Metal–Organic Framework Membrane for Fast and Selective Lithium-Ion Separation. *Angew. Chem., Int. Ed.* **2016**, *55* (48), 15120–15124.

(4) Zavahir, S.; Elmakki, T.; Gulied, M.; Ahmad, Z.; Al-Sulaiti, L.; Shon, H. K.; Chen, Y.; Park, H.; Batchelor, B.; Han, D. S. A review on lithium recovery using electrochemical capturing systems. *Desalination* **2021**, *500* (15), No. 114883.

(5) Liu, S.; Tong, X.; Huang, L.; Xiao, C.; Zhang, K.; Chen, Y.; Crittenden, J. Lithium-ion extraction using electro-driven freestanding graphene oxide composite membranes. *J. Membr. Sci.* **2023**, *672* (15), No. 121448.

(6) Razmjou, A.; Eshaghi, G.; Orooji, Y.; Hosseini, E.; Korayem, A. H.; Mohagheghian, F.; Boroumand, Y.; Noorbakhsh, A.; Asadnia, M.; Chen, V. Lithium ion-selective membrane with 2D subnanometer channels. *Water Res.* **2019**, *159* (1), 313–323.

(7) Wang, H.; Zhai, Y.; Li, Y.; Cao, Y.; Shi, B.; Li, R.; Zhu, Z.; Jiang, H.; Guo, Z.; Wang, M.; Chen, L.; Liu, Y.; Zhou, K.-G.; Pan, F.; Jiang, Z. Covalent organic framework membranes for efficient separation of monovalent cations. *Nat. Commun.* **2022**, *13* (1), No. 7123.

(8) Bian, S.; Li, D.; Gao, D.; Peng, J.; Dong, Y.; Li, W. Hydrometallurgical processing of lithium, potassium, and boron for the comprehensive utilization of Da Qaidam lake brine via natural evaporation and freezing. *Hydrometallurgy* **2017**, *173*, 80−83.
(9) Shi, C.; Jing, Y.; Jia, Y. Solvent extraction of lithium ions by tri-n-butyl phosphate using a room temperature ionic liquid. *J. Mol. Liq.* **2016**, *215*, 640−646.
(10) Tsuchiya, S.; Nakatani, Y.; Ibrahim, R.; Ogawa, S. Highly Efficient Separation of Lithium Chloride from Seawater. *J. Am. Chem. Soc.* **2002**, *124* (18), 4936−4937.
(11) Liu, X.; Chen, X.; He, L.; Zhao, Z. Study on extraction of lithium from salt lake brine by membrane electrolysis. *Desalination* **2015**, *376*, 35−40.
(12) Xu, S.; Song, J.; Bi, Q.; Chen, Q.; Zhang, W.-M.; Qian, Z.; Zhang, L.; Xu, S.; Tang, N.; He, T. Extraction of lithium from Chinese salt-lake brines by membranes: Design and practice. *J. Membr. Sci.* **2021**, *635* (15), No. 119441.
(13) Yu, D.; Xiao, X.; Shokoohi, C.; Wang, Y.; Sun, L.; Juan, Z.; Kipper, M. J.; Tang, J.; Huang, L.; Han, G. S.; Jung, H. S.; Chen, J. Recent Advances in Stimuli-Responsive Smart Membranes for Nanofiltration. *Adv. Funct. Mater.* **2023**, *33* (9), No. 2211983.
(14) Butt, F. S.; Lewis, A.; Chen, T.; Mazlan, N. A.; Wei, X.; Hayer, J.; Chen, S.; Han, J.; Yang, Y.; Yang, S.; Huang, Y. Lithium Harvesting from the Most Abundant Primary and Secondary Sources: A Comparative Study on Conventional and Membrane Technologies. *Membranes* **2022**, *12* (4), No. 373, DOI: 10.3390/membranes12040373.
(15) Liu, G.; Jin, W.; Xu, N. Membranen aus zweidimensionalen Materialien: eine neue Familie hochleistungsfähiger Trennmembranen. *Angew. Chem.* **2016**, *128* (43), 13580−13595.
(16) Han, Z.; Xiao, X.; Qu, H.; Hu, M.; Au, C.; Nashalian, A.; Xiao, X.; Wang, Y.; Yang, L.; Jia, F.; Wang, T.; Ye, Z.; Servati, P.; Huang, L.; Zhu, Z.; Tang, J.; Chen, J. Ultrafast and Selective Nanofiltration Enabled by Graphene Oxide Membranes with Unzipped Carbon Nanotube Networks. *ACS Appl. Mater. Interfaces* **2022**, *14* (1), 1850−1860.
(17) Jia, F.; Xiao, X.; Nashalian, A.; Shen, S.; Yang, L.; Han, Z.; Qu, H.; Wang, T.; Ye, Z.; Zhu, Z.; Huang, L.; Wang, Y.; Tang, J.; Chen, J. Advances in graphene oxide membranes for water treatment. *Nano Res.* **2022**, *15* (7), 6636−6654.
(18) Zhang, Z.; Xiao, X.; Zhou, Y.; Huang, L.; Wang, Y.; Rong, Q.; Han, Z.; Qu, H.; Zhu, Z.; Xu, S.; Tang, J.; Chen, J. Bioinspired Graphene Oxide Membranes with pH-Responsive Nanochannels for High-Performance Nanofiltration. *ACS Nano* **2021**, *15* (8), 13178−13187.
(19) Wang, S.; Yang, L.; He, G.; Shi, B.; Li, Y.; Wu, H.; Zhang, R.; Nunes, S.; Jiang, Z. Two-dimensional nanochannel membranes for molecular and ionic separations. *Chem. Soc. Rev.* **2020**, *49* (4), 1071−1089.
(20) Yan, X.; Xiao, X.; Au, C.; Mathur, S.; Huang, L.; Wang, Y.; Zhang, Z.; Zhu, Z.; Kipper, M. J.; Tang, J.; Chen, J. Electrospinning nanofibers and nanomembranes for oil/water separation. *J. Mater. Chem. A* **2021**, *9* (38), 21659−21684.
(21) Yeh, C.-N.; Raidongia, K.; Shao, J.; Yang, Q.-H.; Huang, J. On the origin of the stability of graphene oxide membranes in water. *Nat. Chem.* **2015**, *7* (2), 166−170.
(22) Zhang, Y.; Zhang, S.; Chung, T.-S. Nanometric Graphene Oxide Framework Membranes with Enhanced Heavy Metal Removal via Nanofiltration. *Environ. Sci. Technol.* **2015**, *49* (16), 10235−10242.
(23) Liu, T.; Zhang, X.; Liang, J.; Liang, W.; Qi, W.; Tian, L.; Qian, L.; Li, Z.; Chen, X. Ultraflat Graphene Oxide Membranes with Newton-Ring Prepared by Vortex Shear Field for Ion Sieving. *Nano Lett.* **2023**, *23*, 9641.
(24) Thebo, K. H.; Qian, X.; Zhang, Q.; Chen, L.; Cheng, H.-M.; Ren, W. Highly stable graphene-oxide-based membranes with superior permeability. *Nat. Commun.* **2018**, *9* (1), No. 1486.
(25) Lu, Z.; Wu, Y.; Ding, L.; Wei, Y.; Wang, H. A Lamellar MXene ($Ti_3C_2T_x$)/PSS Composite Membrane for Fast and Selective Lithium-Ion Separation. *Angew. Chem., Int. Ed.* **2021**, *60* (41), 22265−22269.
(26) Xiong, S.; Qian, X.; Zhong, Z.; Wang, Y. Atomic layer deposition for membrane modification, functionalization and preparation: A review. *J. Membr. Sci.* **2022**, *658*, No. 120740.
(27) Liu, T.; Li, Z.; Zhang, X.; Tan, H.; Chen, Z.; Wu, J.; Chen, J.; Qiu, H. Metal−Organic Framework-Intercalated Graphene Oxide Membranes for Selective Separation of Uranium. *Anal. Sci.* **2021**, *93* (48), 16175−16183.
(28) Liu, G.; Jin, W.; Xu, N. Graphene-based membranes. *Chem. Soc. Rev.* **2015**, *44* (15), 5016−5030.
(29) Qian, J.; Gao, X.; Pan, B. Nanoconfinement-Mediated Water Treatment: From Fundamental to Application. *Environ. Sci. Technol.* **2020**, *54* (14), 8509−8526.
(30) Agrawal, K. V.; Shimizu, S.; Drahushuk, L. W.; Kilcoyne, D.; Strano, M. S. Observation of extreme phase transition temperatures of water confined inside isolated carbon nanotubes. *Nat. Nanotechnol.* **2017**, *12* (3), 267−273.
(31) Fumagalli, L.; Esfandiar, A.; Fabregas, R.; Hu, S.; Ares, P.; Janardanan, A.; Yang, Q.; Radha, B.; Taniguchi, T.; Watanabe, K.; Gomila, G.; Novoselov, K. S.; Geim, A. K. Anomalously low dielectric constant of confined water. *Science* **2018**, *360* (6395), 1339−1342.
(32) Fan, J.; Wu, H.; Wang, F. Evaporation-driven liquid flow through nanochannels. *Phys. Fluids* **2020**, *32* (1), No. 012001.
(33) Zhang, H.; Hou, J.; Hu, Y.; Wang, P.; Ou, R.; Jiang, L.; Liu, J. Z.; Freeman, B. D.; Hill, A. J.; Wang, H. Ultrafast selective transport of alkali metal ions in metal organic frameworks with subnanometer pores. *Sci. Adv.* **2018**, *4* (2), No. eaaq0066.
(34) Saliba, D.; Ammar, M.; Rammal, M.; Al-Ghoul, M.; Hmadeh, M. Crystal Growth of ZIF-8, ZIF-67, and Their Mixed-Metal Derivatives. *J. Am. Chem. Soc.* **2018**, *140* (5), 1812−1823.
(35) Hecht, H.; Srebnik, S. Structural Characterization of Sodium Alginate and Calcium Alginate. *Biomacromolecules* **2016**, *17* (6), 2160−2167.
(36) Wang, J.; Zhang, Z.; Zhu, J.; Tian, M.; Zheng, S.; Wang, F.; Wang, X.; Wang, L. Ion sieving by a two-dimensional $Ti_3C_2T_x$ alginate lamellar membrane with stable interlayer spacing. *Nat. Commun.* **2020**, *11* (1), No. 3540.
(37) Rhim, J.-W. Physical and mechanical properties of water resistant sodium alginate films. *LWT—Food Sci. Technol.* **2004**, *37* (3), 323−330.
(38) Jiao, C.; Xiong, J.; Tao, J.; Xu, S.; Zhang, D.; Lin, H.; Chen, Y. Sodium alginate/graphene oxide aerogel with enhanced strength−toughness and its heavy metal adsorption study. *Int. J. Biol. Macromol.* **2016**, *83*, 133−141.
(39) Qu, H.; Xiao, X.; Han, Z.; Hu, M.; Shen, S.; Yang, L.; Jia, F.; Wang, T.; Ye, Z.; Sun, W.; Wang, Y.; Huang, L.; Zhu, Z.; Servati, P.; Tang, J.; Chen, J. Graphene Oxide Nanofiltration Membrane Based on Three-Dimensional Size-Controllable Metal−Organic Frameworks for Water Treatment. *ACS Appl. Nano Mater.* **2022**, *5* (4), 5196−5207.
(40) Liang, J.; Zhang, X.; Liu, T.-q.; Gao, X.-d.; Liang, W.-b.; Qi, W.; Qian, L.-j.; Li, Z.; Chen, X.-m. Macroscopic Heterostructure Membrane of Graphene Oxide/Porous Graphene/Graphene Oxide for Selective Separation of Deuterium Water from Natural Water. *Adv. Mater.* **2022**, *34* (49), No. 2206524.
(41) Zhu, M.; Venna, S. R.; Jasinski, J. B.; Carreon, M. A. Room-Temperature Synthesis of ZIF-8: The Coexistence of ZnO Nanoneedles. *Chem. Mater.* **2011**, *23* (16), 3590−3592.
(42) Kwon, H. T.; Jeong, H.-K.; Lee, A. S.; An, H. S.; Lee, J. S. Heteroepitaxially Grown Zeolitic Imidazolate Framework Membranes with Unprecedented Propylene/Propane Separation Performances. *J. Am. Chem. Soc.* **2015**, *137* (38), 12304−12311.
(43) Bendejacq, D.; Ponsinet, V.; Joanicot, M.; Loo, Y. L.; Register, R. A. Well-Ordered Microdomain Structures in Polydisperse Poly(styrene)−Poly(acrylic acid) Diblock Copolymers from Controlled Radical Polymerization. *Macromolecules* **2002**, *35* (17), 6645−6649.
(44) Lopes, W. A.; Jaeger, H. M. Hierarchical self-assembly of metal nanostructures on diblock copolymer scaffolds. *Nature* **2001**, *414* (6865), 735−738.

https://doi.org/10.1021/jacsau.3c00473
JACS Au 2023, 3, 3089−3100

(45) Zheng, H.; Yang, J.; Han, S. The synthesis and characteristics of sodium alginate/graphene oxide composite films crosslinked with multivalent cations. *J. Appl. Polym. Sci.* **2016**, *133* (27), No. 43616, DOI: 10.1002/app.43616.
(46) Tao, E.; Ma, D.; Yang, S.; Hao, X. Graphene oxide-montmorillonite/sodium alginate aerogel beads for selective adsorption of methylene blue in wastewater. *J. Alloys Compd.* **2020**, *832*, No. 154833.
(47) Acik, M.; Lee, G.; Mattevi, C.; Pirkle, A.; Wallace, R. M.; Chhowalla, M.; Cho, K.; Chabal, Y. The Role of Oxygen during Thermal Reduction of Graphene Oxide Studied by Infrared Absorption Spectroscopy. *J. Phys. Chem. C* **2011**, *115* (40), 19761−19781.
(48) Nie, L.; Liu, C.; Wang, J.; Shuai, Y.; Cui, X.; Liu, L. Effects of surface functionalized graphene oxide on the behavior of sodium alginate. *Carbohydr. Polym.* **2015**, *117*, 616−623.
(49) Li, Y.; Zhang, X.; Yang, A.; Jiang, C.; Zhang, G.; Mao, J.; Meng, Q. Polyphenol etched ZIF-8 modified graphene oxide nanofiltration membrane for efficient removal of salts and organic molecules. *J. Membr. Sci.* **2021**, *635*, No. 119521.
(50) Fan, J.; Shi, Z.; Lian, M.; Li, H.; Yin, J. Mechanically strong graphene oxide/sodium alginate/polyacrylamide nanocomposite hydrogel with improved dye adsorption capacity. *J. Mater. Chem. A* **2013**, *1* (25), 7433−7443.
(51) Wu, J.-B.; Lin, M.-L.; Cong, X.; Liu, H.-N.; Tan, P.-H. Raman spectroscopy of graphene-based materials and its applications in related devices. *Chem. Soc. Rev.* **2018**, *47* (5), 1822−1873.
(52) Chang, X.; Hu, P.; Liu, H.; Lv, Z.; Yang, J.; Wang, J.; Li, Z.; Qian, L.; Wu, W. ZIF-8 modified graphene oxide/sodium alginate 3D elastic spheres for uranium trapping in seawater. *Desalination* **2023**, *549*, No. 116371.
(53) Ionita, M.; Pandele, M. A.; Iovu, H. Sodium alginate/graphene oxide composite films with enhanced thermal and mechanical properties. *Carbohydr. Polym.* **2013**, *94* (1), 339−344.
(54) Liang, J.; Liu, T.; Li, Y.; Liang, W.; Zhang, X.; Qian, L.; Li, Z.; Chen, X. 2D vertical heterostructure membranes for lanthanide separation. *Cell Rep. Phys. Sci.* **2022**, *3* (3), No. 100769.
(55) Al-Gaashani, R.; Najjar, A.; Zakaria, Y.; Mansour, S.; Atieh, M. A. XPS and structural studies of high quality graphene oxide and reduced graphene oxide prepared by different chemical oxidation methods. *Ceram. Int.* **2019**, *45* (11), 14439−14448.
(56) Fu, J.; Wang, X.; Wang, T.; Zhang, J.; Guo, S.; Wu, S.; Zhu, F. Covalent Functionalization of Graphene Oxide with a Presynthesized Metal−Organic Framework Enables a Highly Stable Electrochemical Sensing. *ACS Appl. Mater. Interfaces* **2019**, *11* (36), 33238−33244.
(57) Tian, F.; Cerro, A. M.; Mosier, A. M.; Wayment-Steele, H. K.; Shine, R. S.; Park, A.; Webster, E. R.; Johnson, L. E.; Johal, M. S.; Benz, L. Surface and Stability Characterization of a Nanoporous ZIF-8 Thin Film. *J. Phys. Chem. C* **2014**, *118* (26), 14449−14456.
(58) Liu, Y.; He, S.; Huang, B.; Kong, Z.; Guan, L. Influence of different Fe doping strategies on modulating active sites and oxygen reduction reaction performance of Fe, N-doped carbonaceous catalysts. *J. Energy Chem.* **2022**, *70*, 511−520.
(59) Wu, T.; Wang, Z.; Lu, Y.; Liu, S.; Li, H.; Ye, G.; Chen, J. Graphene Oxide Membranes for Tunable Ion Sieving in Acidic Radioactive Waste. *Adv. Sci.* **2021**, *8* (7), No. 2002717.
(60) Zhao, H.; Yang, J.; Li, Z.; Geng, Y.; He, S.; Chen, M.; Li, R.; Li, Q.; Zhang, L. Effect of cations on stabilizing graphene oxide membranes in aqueous solutions. *Appl. Surf. Sci.* **2019**, *487*, 962−971.
(61) Wan, S.; Li, X.; Wang, Y.; Chen, Y.; Xie, X.; Yang, R.; Tomsia, A. P.; Jiang, L.; Cheng, Q. Strong sequentially bridged MXene sheets. *Proc. Natl. Acad. Sci. U.S.A.* **2020**, *117* (44), 27154−27161.
(62) He, M.-Y.; Luo, C.-G.; Yang, H.-J.; Kong, F.-C.; Li, Y.-L.; Deng, L.; Zhang, X.-Y.; Yang, K.-Y. Sources and a proposal for comprehensive exploitation of lithium brine deposits in the Qaidam Basin on the northern Tibetan Plateau, China: Evidence from Li isotopes. *Ore Geol. Rev.* **2020**, *117*, No. 103277.
(63) Wang, Y.; Zhang, W.; Zeng, X.; Deng, T.; Wang, J. Membranes for separation of alkali/alkaline earth metal ions: A review. *Sep. Purif. Technol.* **2021**, *278*, No. 119640.
(64) Lu, Z.; Wu, Y.; Ding, L.; Wei, Y.; Wang, H. A Lamellar MXene (Ti3C2Tx)/PSS Composite Membrane for Fast and Selective Lithium-Ion Separation. *Angew. Chem.* **2021**, *133* (41), 22439−22443.
(65) Zhao, Y.; Zhou, C.; Wang, J.; Liu, H.; Xu, Y.; Seo, J. W.; Shen, J.; Gao, C.; Van der Bruggen, B. Formation of morphologically confined nanospaces via self-assembly of graphene and nanospheres for selective separation of lithium. *J. Mater. Chem. A* **2018**, *6* (39), 18859−18864.
(66) Xu, R.; Kang, Y.; Zhang, W.; Zhang, X.; Pan, B. Oriented UiO-67 Metal−Organic Framework Membrane with Fast and Selective Lithium-Ion Transport. *Angew. Chem., Int. Ed.* **2022**, *134* (3), No. e202115443.
(67) Xi, Y.-H.; Liu, Z.; Ji, J.; Wang, Y.; Faraj, Y.; Zhu, Y.; Xie, R.; Ju, X.-J.; Wang, W.; Lu, X.; Chu, L.-Y. Graphene-based membranes with uniform 2D nanochannels for precise sieving of mono-/multi-valent metal ions. *J. Membr. Sci.* **2018**, *550*, 208−218.
(68) Arshadi, F.; Mohammad, M.; Hosseini, E.; Ahmadi, H.; Asadnia, M.; Orooji, Y.; Korayem, A. H.; Noorbakhsh, A.; Razmjou, A. The effect of D-spacing on the ion selectivity performance of MXene membrane. *J. Membr. Sci.* **2021**, *639*, No. 119752.
(69) Abdollahzadeh, M.; Chai, M.; Hosseini, E.; Zakertabrizi, M.; Mohammad, M.; Ahmadi, H.; Hou, J.; Lim, S.; Habibnejad Korayem, A.; Chen, V.; Asadnia, M.; Razmjou, A. Designing Angstrom-Scale Asymmetric MOF-on-MOF Cavities for High Monovalent Ion Selectivity. *Adv. Mater.* **2022**, *34* (9), No. 2107878.
(70) Xin, W.; Lin, C.; Fu, L.; Kong, X.-Y.; Yang, L.; Qian, Y.; Zhu, C.; Zhang, Q.; Jiang, L.; Wen, L. Nacre-like Mechanically Robust Heterojunction for Lithium-Ion Extraction. *Matter* **2021**, *4* (2), 737−754.
(71) Tan, R.; Wang, A.; Malpass-Evans, R.; Williams, R.; Zhao, E. W.; Liu, T.; Ye, C.; Zhou, X.; Darwich, B. P.; Fan, Z.; Turcani, L.; Jackson, E.; Chen, L.; Chong, S. Y.; Li, T.; Jelfs, K. E.; Cooper, A. I.; Brandon, N. P.; Grey, C. P.; McKeown, N. B.; Song, Q. Hydrophilic microporous membranes for selective ion separation and flow-battery energy storage. *Nat. Mater.* **2020**, *19* (2), 195−202.
(72) Zhang, W.; Huang, Q.; Liu, S.; Zhang, M.; Liu, G.; Ma, Z.; Jin, W. Graphene oxide membrane regulated by surface charges and interlayer channels for selective transport of monovalent ions over divalent ions. *Sep. Purif. Technol.* **2022**, *291*, No. 120938.
(73) Cheng, L.; Guo, Y.; Liu, Q.; Liu, G.; Li, R.; Chen, X.; Zeng, H.; Liu, G.; Jin, W. Metal Confined in 2D Membranes for Molecular Recognition and Sieving towards Ethylene/Ethane Separation. *Adv. Mater.* **2022**, *34* (44), No. 2206349.
(74) Chen, L.; Shi, G.; Shen, J.; Peng, B.; Zhang, B.; Wang, Y.; Bian, F.; Wang, J.; Li, D.; Qian, Z.; Xu, G.; Liu, G.; Zeng, J.; Zhang, L.; Yang, Y.; Zhou, G.; Wu, M.; Jin, W.; Li, J.; Fang, H. Ion sieving in graphene oxide membranes via cationic control of interlayer spacing. *Nature* **2017**, *550* (7676), 380−383.
(75) Marcano, D. C.; Kosynkin, D. V.; Berlin, J. M.; Sinitskii, A.; Sun, Z.; Slesarev, A.; Alemany, L. B.; Lu, W.; Tour, J. M. Improved Synthesis of Graphene Oxide. *ACS Nano* **2010**, *4* (8), 4806−4814.
(76) Wang, Z.; Huang, L.; Dong, X.; Wu, T.; Qing, Q.; Chen, J.; Lu, Y.; Xu, C. Ion sieving in graphene oxide membrane enables efficient actinides/lanthanides separation. *Nat. Commun.* **2023**, *14* (1), No. 261.
(77) Li, Z.; Zhang, X.; Tan, H.; Qi, W.; Wang, L.; Ali, M. C.; Zhang, H.; Chen, J.; Hu, P.; Fan, C.; Qiu, H. Combustion Fabrication of Nanoporous Graphene for Ionic Separation Membranes. *Adv. Funct. Mater.* **2018**, *28* (43), No. 1805026.